Article

Switching of Transfer Characteristics of an Organic Field-Effect Transistor by Phase Transitions: Sensitive Response to Molecular Dynamics and Charge Fluctuation

Seiya Yokokura, Yukihiro Takahashi, Hiroki Nonaka, Hiroyuki Hasegawa, Jun Harada, Tamotsu Inabe, Reiji Kumai, Hiroshi Okamoto, Michio M. Matsushita, and Kunio Awaga

Chem. Mater., **Just Accepted Manuscript** • DOI: 10.1021/acs.chemmater.5b01383 • Publication Date (Web): 27 May 2015

Switching of Transfer Characteristics of an Organic Field-Effect Transistor by Phase Transitions: Sensitive Response to Molecular Dynamics and Charge Fluctuation

Seiya Yokokura,[1] Yukihiro Takahashi, [*,1,2,3] Hiroki Nonaka,[4] Hiroyuki Hasegawa,[1,2,3] Jun Harada,[1,2,3] Tamotsu Inabe,[*,1,2,3] Reiji Kumai,[5] Hiroshi Okamoto,[4] Michio M. Matsushita,[3,6] and Kunio Awaga[3,6]

[1]*Graduate School of Chemical Sciences and Engineering, Hokkaido University, Sapporo 060-0810, Japan*

[2]*Department of Chemistry, Faculty of Science, Hokkaido University, Sapporo 060-0810, Japan*

[3]*JST, CREST, Chiyoda-Ku, Tokyo 102-0076, Japan*

[4]*Department of Advanced Materials Science, The University of Tokyo, Chiba 277-8561, Japan*

[5]*Condensed Matter Research Center (CMRC) and Photon Factory, High Energy Accelerator Research Organization (KEK), Institute of Materials Structure Science, Tsukuba 305-0801, Japan*

[6]*Department of Chemistry and Research Center for Materials Science, Nagoya University, Nagoya 464-8602, Japan*

ABSTRACT: An organic field-effect transistor was fabricated using an anthracene–tetracyanoquinodimethane (AN–TCNQ) single-crystal charge-transfer (CT) complex as the semiconductor material. The CT complex showed molecular dynamics related to reorientational motion of AN molecule at room temperature. The transfer characteristics drastically changed when the temperature decreased from room temperature to 90 K: n-type → ambipolar-type → p-type → ambipolar-type. From thermal analysis, AN–TCNQ underwent two phase transitions when the temperature decreased from room temperature to 120 K. To clarify the mechanism of the drastic changes of the transfer characteristics, the crystal and electronic structures of AN–TCNQ at various temperatures were investigated by X-ray structure analysis, optical measurements, and magnetic measurements. It was found that the drastic changes of the transfer characteristics originated from changes in the electronic structure accompanied by the molecular dynamics.

1. INTRODUCTION

Recently, a wide variety of organic-based field-effect transistors (FETs) have been fabricated and investigated.[1-6] Their performance has been improved in various studies, and many organic-based devices exceeding the performance of amorphous silicon have been reported.[7-16] Some of them show high performance even in thin film transistors, having attractive features for ubiquitous network such as low-cost, flexibility, or large area.[3-12] In general, the performance of organic FETs depends on the crystal and band structures of the semiconductor layers. The mobility of devices is dominated by electronic structures of the semiconductor materials, which depend on the intermolecular interaction. Therefore, FETs sense the change of electronic structure of semiconductor layer. For example, the transfer characteristics of FETs change largely by a slight change of the electronic or band structure of semiconductor layers by contacting and adsorbing the gases.[17-21] FETs can detect slight change of electronic structure of semiconductor materials by external stimuli and the device property change largely. In this study, we fabricated FET using charge-transfer complex crystal as semiconductor layer, which showed switching between n-type and p-type in transfer characteristics by decreasing temperature.

Charge-transfer (CT) complexes consist of an electron donor and acceptor. The crystals of CT complexes are of great interest and importance in the field of molecular materials, showing high electronic conductivity and superconductivity.[22-24] These properties are observed in CT crystals with segregated-stacks of donor and acceptor molecules, forming independent π-electron systems based on each component. On the other hand, a CT complex whose donor and acceptor are alternately stacked with face-to-face stacking is classified as a mixed-stacked CT complex. Although crystals with such a molecular arrangement are unable to be a molecular conductor, these complexes can be used as semiconductor layer of FETs.[25-27] In this study, we designed a molecular electronic system in which molecular dynamics in a mixed-stack CT complex is closely connected with the property of FET.

In mixed-stack CT complexes, molecular dynamics such as in-plane reorientation occurs with using planer molecules as donor such as anthracene–tetracyanobenzene, pyrene–tetracyanobenzene and pyrene–pyromellitic-dianhydride.[28-30] It is known that these

complexes undergo phase transitions at low temperature, which are related to the order–disorder behavior of molecular orientation of these molecules.[31] The reorientational motion causes change of relative orientation of donor and acceptor molecules. The relative orientation is important in CT crystals since the CT interactions occur by overlap of π-orbitals of these molecules. In such crystals, it is expected that the CT interactions and electronic structures change by reorietational motion. We consider that FETs can detect the changes of electronic structure and reorientational motion in CT complex crystals caused by phase transition.

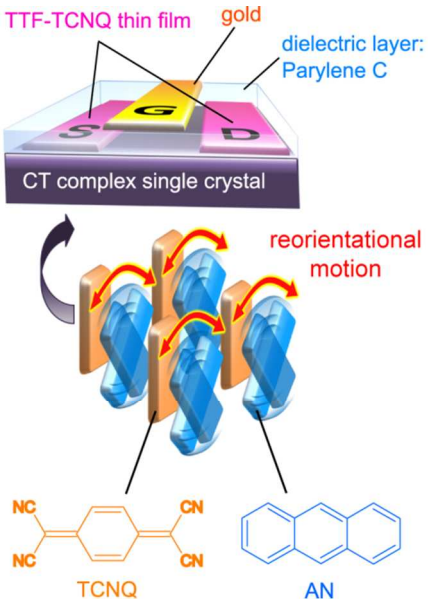

Figure 1. Schematic of the FET (top) and reorientation in the AN–TCNQ crystal (bottom).

In this work, a FET was fabricated utilizing anthracene–tetracyanoquinodimethane (AN-TCNQ) single crystal and tetrathiafulvalene–TCNQ (TTF–TCNQ) metallic thin films as the semiconductor layer and the source and drain electrodes, respectively (Figure 1). AN–TCNQ is a classical CT complex whose crystal structure at room temperature was first reported in 1968.[32] Observed molecular structure of AN showed large atomic displacement parameters (temperature factors), which interpreted as orientational disorder.[31] We have found that the transfer characteristics of the device show drastic changes with decreasing the temperature; n-type → ambipolar-type → p-type → ambipolar-type from room temperature to 90 K. The drastic changes can be explained by molecular dynamics and two structural phase transitions. The results and discussion presented in this paper might give a hint to fabricating the devices that can be switching between n-type and p-type. This study also showed that the measurement of FET characteristics of semiconductor materials is useful to investigate their band and electronic structures.

2. MATERIALS AND METHODS

2.1. Materials. AN, TCNQ and TTF were purchased from Tokyo Chemical Industry Co., Ltd. and purified by vacuum sublimation. Single crystals of the AN–TCNQ complex (black blocks and sticks with a typical size of 0.2 × 0.4 × 1.0 mm^3) were prepared by a co-sublimation method in a sealed vacuum glass tube. The crystal structure of the crystals at room temperature was the same as that in a previous report.[32] TTF–TCNQ polycrystallites were obtained by mixing of each acetone solution of TTF and TCNQ.

2.2. Device Fabrication. Devices with gold or silver as the source and drain electrodes were fabricated, but their transfer characteristics could not be measured at low temperature because of their large contact resistance. To improve the interfacial electrical contact for electron injection into the AN–TCNQ crystals, we used TTF–TCNQ metallic thin films as the source and drain electrodes (Figure 1). By thermal evaporation through shadow masks, metallic thin films were deposited on the (110) plane of a bulk single crystal of AN–TCNQ whose thickness was 200 μm. The channel width and length (W and L) of the obtained device were 675 and 50 μm, respectively. The two electrodes were arranged for the current to flow parallel to the molecular stacking axis of the AN–TCNQ crystal (c axis). A 0.5-μm layer of Parylene C was deposited as the gate dielectric layer (C_i = 5.1 nF/cm^2). Gold gate electrodes were then formed on the top of the insulator layer.

2.3. Crystallographic Study. All of the diffraction measurements were performed on a Bruker SMART APEX II ULTRA diffractometer with a TXS rotating anode (Mo Kα radiation, λ = 0.71073 Å) and multilayer optics. The data collection was carried out using a DX-CS190LD N_2-gas-flow cryostat (Japan Thermal Engineering, Sagamihara, Japan). The temperature in the nozzle was kept constant within ±0.2 K during the measurement. Low-temperature measurements were performed at cooling process using the same crystal. The structures were solved by direct methods (SHELXT) and refined by full-matrix least-squares on F^2 using SHELXL-2014.[33] All of the H atoms were refined using a riding model. For the crystal structures without disorder, all of the non-H atoms were refined anisotropically. For the crystal structures with disorder, details of the refinement are provided in the Supporting Information as CIF files embedding the SHELXL-2014 res files. The crystal and experimental data are summarized in Table 1.

2.4. Calculation. The overlap integrals between the highest occupied molecular orbital (HOMO) and next HOMO (nHOMO) of AN and the lowest unoccupied molecular orbital (LUMO) of TCNQ for each phase were calculated under the extended Hückel approximation[34, 35] using the CAESAR program package.[36] The optimization and energy calculations of isolated single molecules were performed using Gaussian 09W at the B3LYP/6-31G(d,p) level.[37]

2.5. Measurements. The device properties of the AN–TCNQ single-crystal FET were measured using a dual channel system source meter (Keithley 2636A). Temperature was controlled using a closed cycle cryostat system. Thermal analyses were performed by differential scanning calorimetry (DSC, Mettler Toledo Thermal Analysis

Table 1. Crystallographic Data for Each Phase of AN–TCNQ

	300 K	155 K	100 K
formula		C26 H14 N4	
formula weight		382.41	
crystal size (mm^3)		0.30 × 0.20 × 0.20	
crystal system	monoclinic	monoclinic	triclinic
space group	*C*2/*m*	$P2_1/a$	*P*–1
a (Å)	11.5276(3)	11.5730(15)	11.370(3)
b (Å)	12.9749(4)	12.8479(16)	12.818(3)
c (Å)	7.0126(2)	6.9092(9)	6.9180(17)
α (°)	90	90	90.884(4)
β (°)	105.5838(14)	107.053(2)	107.171(4)
γ (°)	90	90	94.998(4)
V ($Å^3$)	1010.31(5)	982.2(2)	958.8(4)
Z	2	2	2
R_{int}	0.0166	0.0317	0.0312
goodness-of-fit on F^2	1.069	1.094	1.061
R_1 [$I > 2\sigma(I)$]	0.0452	0.0413	0.0449
R_w (all reflection)	0.1477	0.1331	0.1174

Table 2. Temperature Dependence of the Mobility in the AN–TCNQ FET

	300 K	250 K	220 K	200 K	150 K	100 K
μ_n ($cm^2/(V{\cdot}s)$)	4.5×10^{-5}	2.4×10^{-6}	3.2×10^{-7}	7.1×10^{-7}	-	6.2×10^{-8}
μ_p ($cm^2/(V{\cdot}s)$)	-	1.5×10^{-6}	5.7×10^{-7}	5.3×10^{-7}	5.0×10^{-7}	1.2×10^{-8}

System, DSC 1) with a heating and cooling rate of 5 K/min. The DSC profile was confirmed to be reproduced in the repeated thermal cycles. To obtain the polarized reflectivity (*R*) of AN–TCNQ in the ultraviolet–visible (UV/vis) and infrared (IR) regions, we used a specially designed spectrometer with a 25-cm-grating monochromator (JASCO M25-GT) and an optical microscope and a Fourier transform IR spectrometer with an optical microscope, respectively. In the low-temperature measurements, a specially designed conduction-type cryostat was used. Magnetic susceptibility measurements were performed on a Quantum Design MPMS superconducting quantum interference device (SQUID) susceptometer with a static field of 1 T in the temperature range 2–300 K using randomly oriented polycrystalline sample. The diamagnetic core contribution was estimated based on Pascal's constants.[38]

3. RESULTS AND DISCUSSION

3.1. Field-Effect Transistor of AN–TCNQ Single Crystal. Figure 2 shows the device properties of the AN–TCNQ single-crystal FET in variable temperatures. The device showed typical n-type behavior at 300 K, where the drain current (I_{SD}) is enhanced by positive gate voltage (V_G). The device exhibited normally on behavior, the threshold voltage (V_{th}) was –20.2 V. The mobility μ was estimated 4.5×10^{-5} $cm^2/(V{\cdot}s)$ applying the formula $\mu = (dI_{SD}/dV_G) \times [L/(WC_iV_D)]$ to the linear region of transfer characteristics. At 250 K, although the dominant carrier was electrons, slight p-type behavior was also observed. The contribution of the p-type behavior of the device became significant than n-type with decreasing temperature: The device became clearly ambipolar at 220 K, and mostly p-type at 200 K, and exclusively p-type at 150 K. However, At 100 K, the device again showed ambipolar-type behavior with a relatively weak p-type contribution. The ambipolar behavior was maintained to the lowest temperature available (90 K). Thus, the transfer characteristics of the AN–TCNQ single-crystal FET drastically changed from n-type → ambipolar-type → p-type → ambipolar-type when the temperature decreased from room temperature to 100 K. The μ values of the n-type (μ_n) and p-type (μ_p) contributions, and the V_{th} values at each temperature are summarized in Table 2.

It is well known that organic FETs show that increase or decrease of mobility by decreasing temperature, but switching between n-type and p-type have never been reported to our knowledge. As shown below, the drastic changes in transfer characteristics of AN-TCNQ FET are

related to the changes of molecular dynamics and electronic structure by two structural phase transitions.

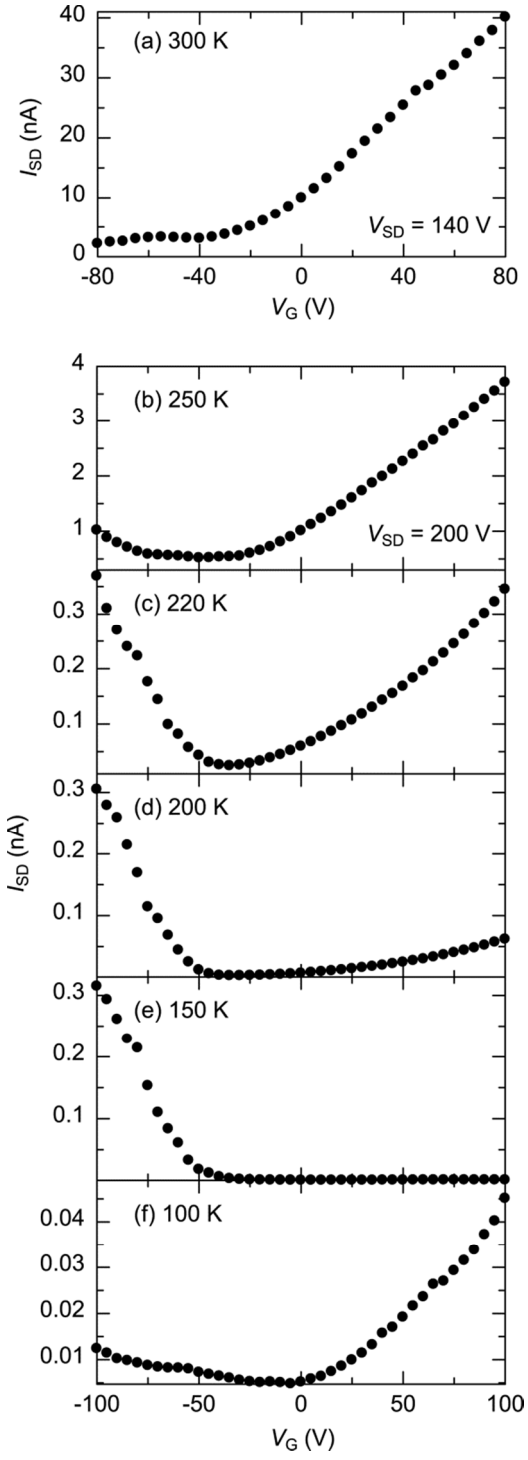

Figure 2. Transfer characteristics of the AN–TCNQ FET at (a) 300 K with V_{SD} = 140 V, (b) 250 K with V_{SD} = 200 V, (c) 220 K with V_{SD} = 200 V, (d) 200 K with V_{SD} = 200 V, (e) 150 K with V_{SD} = 200 V, and (f) 100 K with V_{SD} = 200 V.

3.2. Phase Transitions of AN–TCNQ. DSC measurements show the presence of two reversible structural phase transitions in AN–TCNQ at low temperatures (Figure 3). Two phase transitions are present in both processes (139 K, 160K in heating / 139 K, 161 K in cooling process). The transition enthalpy (entropy) values at low and high temperatures were calculated by integrating the areas of the DSC peaks as ΔH = 0.70 kJ mol^{-1} (ΔS = 5.0 J K^{-1} mol^{-1}) and ΔH = 0.49 kJ mol^{-1} (ΔS = 3.1 J K^{-1} mol^{-1}), respectively. We use the following nomenclature for each phase: HT phase (high-temperature phase, T > 160 K), IM phase (intermediate-temperature phase, 139 K< T <160 K), and LT phase (low-temperature phase, T < 139 K). The relationship between the device behavior and the phase transitions of the AN–TCNQ crystal can be summarized as follows. In the HT phase, with decreasing temperature, the FET of the AN–TCNQ single crystal changed from n-type to p-type behavior via ambipolar behavior (Figure 2a–d). In the IM phase, p-type behavior is maintained (Figure 2e), and the LT phase showed ambipolar behavior (Figure 2f).

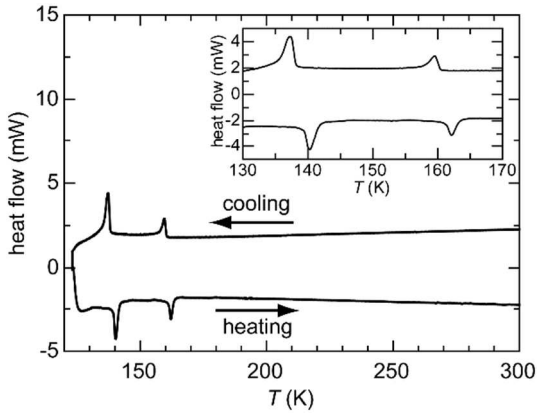

Figure 3. DSC profile of polycrystalline AN–TCNQ. The inset is that around phase transitions.

3.3. Crystal Structures of AN–TCNQ. The crystal structures in the HT (300 K), IM (155 K), and LT (100 K) phases were determined by single-crystal X-ray structure analysis. In HT phase the space group of the crystal is $C2/m$, and each molecule is located on the 2/m sites (Figure 4a). The AN molecules were refined as the overlap of three different orientations, two of which were related to each other by the symmetry of the sites. In these two arrangements (blue and green), the molecular long axes of AN significantly deviate from the mirror plane, while both AN (gray) and TCNQ (orange) share the same mirror plane in another arrangement. The occupancies were refined to be 35.6(17) % (blue and green AN) and 28.8(34) % (gray AN). In the HT phase, it is considered that exchanging of these three orientations occur by in-plane molecular reorientation of AN. All the mixed-stack columns are translationally related with each other.

In IM phase (155 K), the space group of the crystal is $P2_1/a$, which is lower symmetry than the HT phase (Figure 4b). In this space group, mirror symmetry is absent. Although orientational disorder was also observed in this phase, the number of orientation in the IM phase was different to that in the HT phase. There are two orientations of the AN molecule, and the occupancies are refined to be 65.2(13) % (blue AN) and 34.8(13) % (gray AN). The decrease of the number of orientation from three to two at

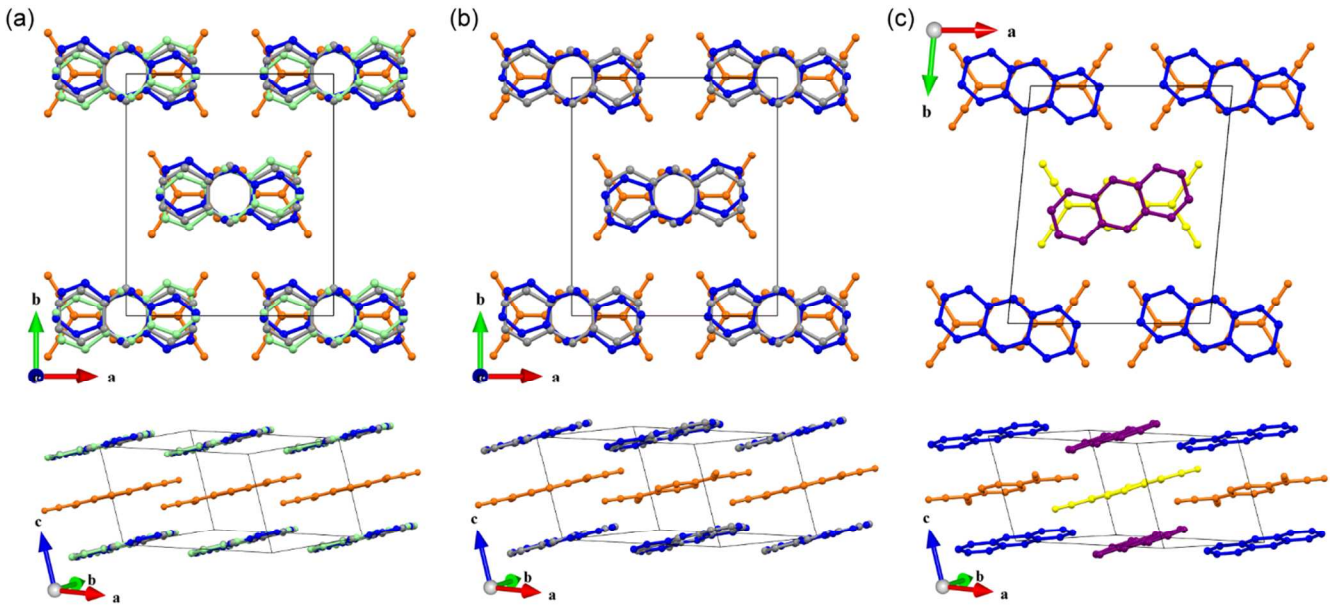

Figure 4. Crystal structures of AN–TCNQ at (a) 300, (b) 155, and (c) 100 K. Each top projection is viewed along the *c* axis, and each bottom perspective view indicates the mixed-stack columns at (0, 0, *z*), (1/2, 1/2, *z*), and (0, 0, *z*).

the phase transition is consistent with the magnitudes of transition entropy, $\Delta S = R \ln(1.45)$ (~$R \ln(3/2)$), where R is the gas constant. The mixed-stack column at (0, 0, *z*) is related by the *a*-glide plane with that at (1/2, 1/2, *z*).

In the LT phase (100 K), the symmetry of the space group of AN–TCNQ is further lowered to *P*–1. Two independent mixed-stacked columns are present in the unit cell (Figure 4c). In Figure 4c, the AN and TCNQ molecules of these columns are either blue AN and orange TCNQ or purple AN and yellow TCNQ. In the LT phase, there is no orientational disorder of AN, suggesting that reorientational motion is suppressed. The magnitude of transition entropy also suggest order–disorder phase transition with two different orientations, $\Delta S = R \ln(1.82)$ (~$R \ln(2)$). The mixed-stack column at (0, 0, *z*) is no longer related with that at (1/2, 1/2, *z*). They are completely independent to each other.

Thus, the AN–TCNQ complex showed two structural phase transitions when the temperature decreased from room temperature to 100 K, and the reorientational motion of AN changed at the phase transition temperatures.

3.4. Molecular Overlap and CT Degree of AN–TCNQ. In this section, the molecular orbitals contributing to carrier transport and the CT degree between AN and TCNQ are discussed based on the geometry obtained from the X-ray structure analyses. As shown in Figure 4a, there are three overlapping modes (OMs) of AN and TCNQ molecules in the HT phase, two OMs in the IM phase, and two OMs in the LT phase. Thus, there are a total of seven OMs. These seven OMs are called OM1 to OM7 (Figure 5b). For these OMs, the overlap integrals between the LUMO of the TCNQ molecule and the HOMO or nHOMO of the AN molecule were calculated. The three molecular orbitals are illustrated in Figure 5a. The overlap integrals and molecular orbitals are summarized in Table 3.

Table 3. Degree of CT and Overlap Integral of Each Overlapping Mode (OM)

	overlapping mode	degree of CT[a]	overlap integral (10^{-3}) HOMO–LUMO
300 K (HT phase)	OM1, 3	0.13	3.5
	OM2		14.3[b]
155 K (IM phase)	OM4	0.08	5.7
	OM5		0.9
100 K (LT phase)	OM6	0.05	8.3
	OM7	0.14	8.7

[a]Degree of CT estimated from the geometry of TCNQ

[b]Overlap integral between nHOMO of AN and LUMO of TCNQ

In the HT phase, three OMs are exchanging in the molecular stacking column by reorientational motion of the AN molecule. The two OMs in which the AN molecule is located out of the TCNQ mirror plane are called OM1 and OM3. In the OM2, both molecules are located in the mirror plane. According to the orthogonality of the HOMO of AN and LUMO of TCNQ, there is no CT interaction in OM2, which was also suggested by Wright.[38] We considered that the CT interaction in OM2 was generated between the nHOMO of AN and the LUMO of TCNQ. The overlap integral in OM2 is 14.3×10^{-3}. However, in OM1 and OM3, CT interaction occurs between the HOMO of AN and the LUMO of TCNQ because the molecular long axis of AN is not located on the TCNQ mirror plane. Because OM1 and OM3 are crystallographically equivalent, the overlap integral for both OM1 and OM3 is the same (3.5×10^{-3}).

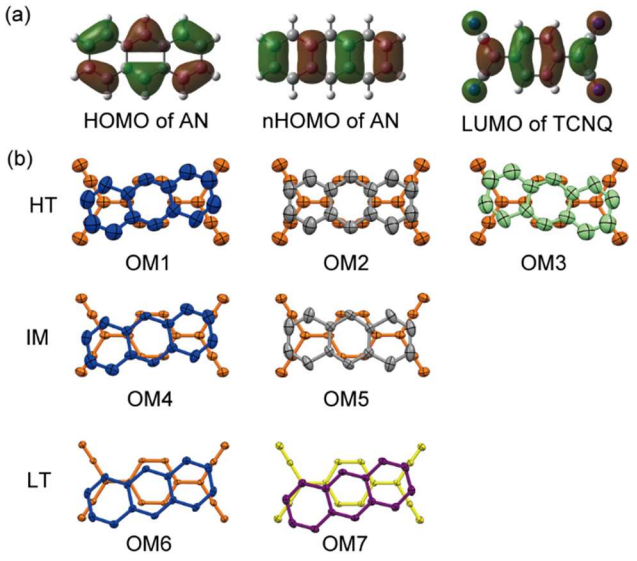

Figure 5. (a) HOMO and nHOMO of the AN molecule, and the LUMO of the TCNQ molecule, which were calculated at the DFT-B3LYP/6-31G(d,p) level. (b) Top views of AN and TCNQ overlap at 300, 155, and 100 K. The ellipsoids are drawn at the 50% probability level.

In the IM phase, there are two OMs (OM4 and OM5) in the crystal. The two OMs are exchanging in the stacking column by reorientation motion of AN. The OM4 is similar to OM1 and OM3, in which the each molecular long axis are crossed. In this OM, a large overlap integral between the HOMO of AN and the LUMO of TCNQ is observed (5.7×10^{-3}). In OM5, the molecular long axes are almost parallel. Although this relative arrangement looks the same as OM2, a non-zero overlap integral between the HOMO of AN and the LUMO of TCNQ is generated in OM5 (0.9×10^{-3}) since the mirror symmetry was extinct in the IM phase.

In the LT phase, the AN molecule does not show orientational disorder. Two OMs (OM6 and OM7) occur for the two crystallographically independent columns. Reorientation from OM6 to OM7 does not occur in a column. Both of the OMs are similar to OM1, OM3, and OM5. The overlap integrals of OM6 and OM7 are 8.3×10^{-3} and 8.7×10^{-3}, respectively.

It is well known that the degree of CT of TCNQ complexes can be estimated using the length of the C=C bond between the dicyanomethylene and quinoid ring in the TCNQ skeleton.[40] The degrees of CT of the seven OMs are also included in Table 3. The degree of CT in the bulk did not significantly change through the two phase transitions. It should be noted that AN–TCNQ takes a neutral ground state in all the phases. The difference between the oxidation potential of AN and the reduction potential of TCNQ (ΔE = 1.2 V) indicates that the electronic state of the complex situates far from the neutral-ionic boundary defined by Torrance.[41] Therefore, it is reasonable that the degree of CT determined from the structural analysis of the balk crystal is nearly zero in all the phases. However, as shown below, a small but important ionic contribution was found to exist.

3.5. Ionic Domains in the AN–TCNQ Crystal. Optical measurements were taken to investigate the electronic state at low temperature. Figure 6a shows the temperature dependence of the reflectivity in the UV/vis and near-IR region with the electric field of light parallel to the π-stacking direction along the *c* axis (perpendicular to the molecular planes). The CT transition from the HOMO of AN to the LUMO of TCNQ (indicated by ♦ in Figure 6a) occurs at around 1.5 eV and that from the nHOMO to the LUMO (□ in Figure 6a) occurs at around 2.6 eV. The intensity of the former peak greatly increases below the second phase transition with decreasing temperature. The transition from the nHOMO to the LUMO shifts to lower energy below the first phase transition with decreasing temperature. Figure 6b shows the spectra with light perpendicular to the stack (*c* axis). In the spectra, a weak peak corresponding to transition from the single-occupied molecular orbital to the LUMO of $TCNQ^{-1}$ (LUMO to next LUMO of TCNQ) is observed around 2.5 eV.[42] This peak might indicate the existence of ionic domains in the crystal even at room temperature. Below 140 K, the peak intensity markedly increases. These results indicate that the electronic state changes at the phase transitions and the ionic character are clearer in the LT phase than in the HT phase.

The degree of CT was investigated by IR spectroscopy. Figure 6c shows the temperature dependence of the reflectivity around 2200 cm^{-1} with the electric field of light perpendicular to the stack (*c* axis). The observed peaks are caused by the IR-active CN stretching (b_{1u}) mode of TCNQ polarized along the long molecular axis. The frequency is known to closely depend on the degree of CT (ρ).[43] As the temperature decreases below 200 K, the single band located at 2218 cm^{-1} splits into two bands, and the lower frequency (higher frequency) band shifts to lower (higher) frequency. This indicates that two types of TCNQ molecules with different ρ values are generated. The blue and red broken lines in Figure 6c show the frequencies of the CN stretching mode for $TCNQ^{0}$ and $TCNQ^{-1}$ determined from the IR spectra of TCNQ and K-TCNQ crystals, respectively.[43, 44] With lowering temperature, the CN stretching mode of $TCNQ^{-1}$ shows a slight higher-frequency shift.[44] We assumed the same magnitude of the temperature-dependent shift for the mode of $TCNQ^{0}$. We determined the ρ values using these two lines assuming a linear relationship between ρ and the frequency, and ρ is plotted as a function of temperature in Figure 6d. Below 200 K, two ρ values appear. As the temperature decreases, the larger value of ρ gradually increases (reaching 0.49 at 20 K), while the smaller value of ρ remains almost constant (~0.25–0.3). These optical measurements suggest that the electronic structure of AN–TCNQ drastically changes at the two phase transitions. Because of large molecular dynamics and one-dimensional fluctuation, a small number of ionic domains are present even at room temperature. Thus, the electronic structure of AN–TCNQ is rather complicated because of the molecular dynamics in the crystal.

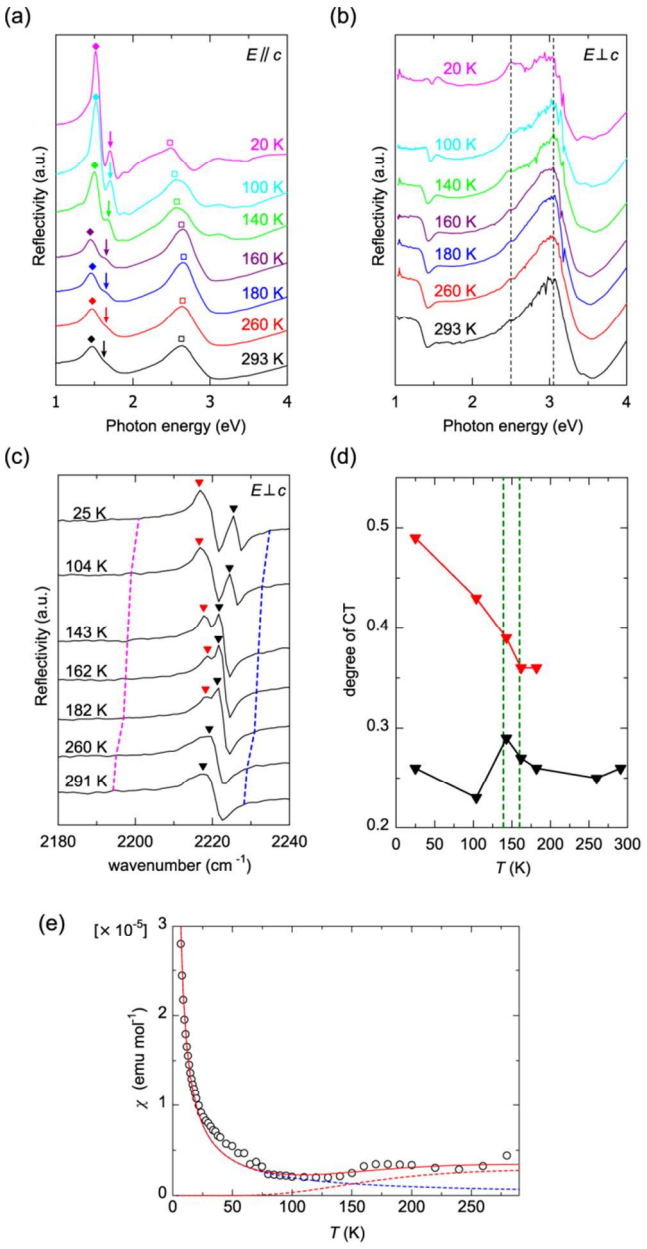

Figure 6. Temperature dependence of the reflectivity spectra of AN–TCNQ polarized (a) parallel to the stack *c* axis and (b) perpendicular to the stack *c* axis. (c) Temperature dependence of the IR reflectance spectra. The polarization direction was perpendicular to the stack *c* axis. The blue and red broken lines show the frequencies of the CN stretching mode of $TCNQ^{0}$ and $TCNQ^{-1}$ at each temperature determined from the IR spectra of TCNQ and K–TCNQ crystals, respectively. (d) Temperature dependence of the degree of CT in AN–TCNQ. The black and red triangles are the degree of CT calculated using the frequency of CN stretching in the IR spectra (black and red triangles in (c), respectively). (e) Magnetic susceptibility of AN–TCNQ. The red dotted line is singlet–triplet fitting, the blue dotted line is Curie fitting, and red solid line is the sum of these two components.

The magnetic susceptibility also indicates the presence of fractional ionic domains in the AN–TCNQ crystal (Figure 6e). Although the magnetic susceptibility of typical neutral mixed-stacked CT complexes only show Curie behavior originating from impurities or defects, the magnetic susceptibility of AN–TCNQ shows a paramagnetic contribution with an anti-ferromagnetic interaction around the phase transition from the HT to the IM phase. This result indicates the presence of ionic domains in the HT and IM phases of the AN–TCNQ crystal. The blue and red dotted lines in Figure 6e show Curie and singlet–triplet fitting, respectively. The Curie constant obtained by fitting was 1.906×10^{-4} emu K mol^{-1} (the spin density was 0.5%), indicating that the Curie component originated from lattice defects. The exchange interaction $|J/k_B|$ and the spin density of the singlet–triplet component were 539 K and 2%, respectively.

Thus, the presence of ionic pairs has been confirmed by optical and magnetic measurements. In the HT and IM phases, the proportion of ionic pairs is 2%. Although the actual number of ionic pairs is difficult to estimate in the LT phase, the results of optical measurements indicate that the density of ionic species gradually increases with decreasing temperature.

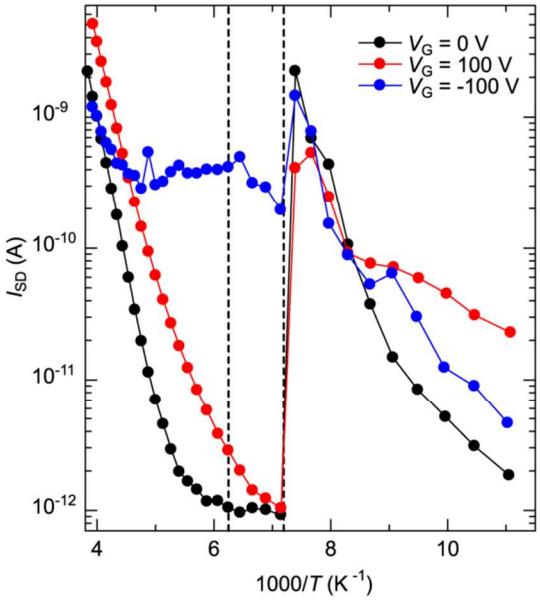

Figure 7. Temperature dependence of I_{SD} with V_G = 0 (black), 100 (red), and –100 V (blue). The two dashed lines indicate the transition temperatures.

3.6. Relationship between the Device Property and Dynamics. Here, we discuss the relationship between the transfer characteristics and molecular dynamics of AN–TCNQ. The I_{SD} values of the AN–TCNQ FET at V_G = 100, 0, and –100 V are plotted against the reciprocal temperature in Figure 7. In the HT phase, the I_{SD} value at V_G = 100 V, which is related to the n-type character, decreases with thermally activated behavior. The thermal activation energy is estimated to be about 0.37 eV. In the IM phase, the activation energy decreases to 0.10 eV, which is considered to be because of the enhancement of the overlap integrals between AN and TCNQ molecules. In the HT phase, the I_{SD} value at V_G = –100 V, which is related to p-type behavior, is almost independent of temperature.

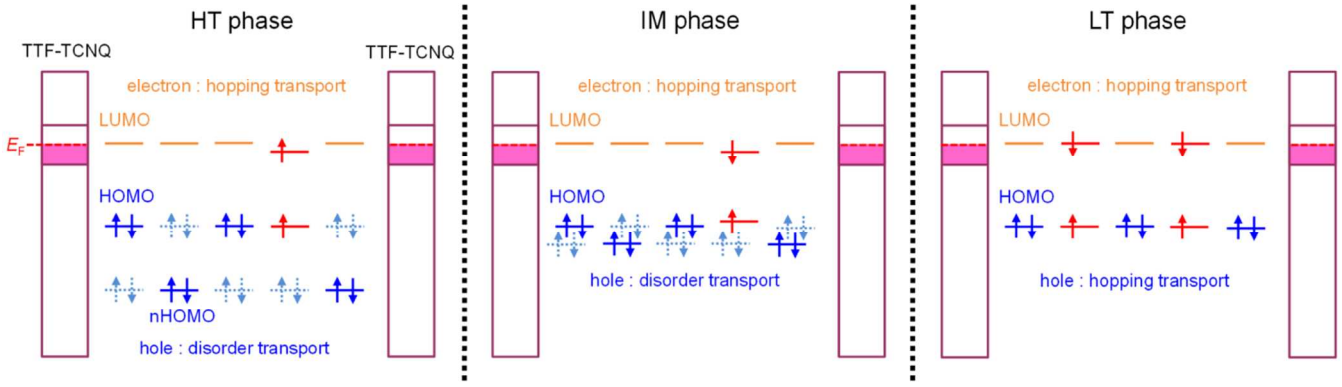

Figure 8. Schematics of the interfaces between the TTF–TCNQ electrodes and AN–TCNQ single crystal in each phase.

In the IM phase, the current gradually decreases with decreasing temperature. Around the phase transition from the IM to the LT phase, both of the I_{SD} values greatly increase. This is considered to be caused by an increase of the ionic domains at the phase transition. After the large increase of the current, the current decreases in accordance with thermal activation. These results indicate that the transport mechanism of the injected holes is different to that of electrons in the HT and IM phases of AN–TCNQ. From the thermally activated behavior, the electron transport mechanism is considered to be hopping between the LUMOs of TCNQ.[45] However, the hole is considered to transport through AN's HOMOs and nHOMOs, which are converting by the reorientational motion of the AN molecule. Thus, the molecular orbitals of the hole transport are dynamically disordered. It is considered that the current in disordered systems flows without temperature dependence.[46]

From these results, the mechanism for the drastic changes of the transfer characteristics of the AN–TCNQ-based FET can be speculated as follows. Schematics of the interface between the TTF–TCNQ electrodes and the AN–TCNQ single crystal in each phase are shown in Figure 8. The band widths of AN–TCNQ, which were calculated in extended Hückel approximation, are quite narrow because of their mixed-stacked arrangement (see Supporting information). Therefore, the band structure of AN–TCNQ can be treated as molecular orbitals. Because TTF–TCNQ used for the electrodes material contains the TCNQ molecule, the Fermi level of the electrodes is located near the LUMO of TCNQ in AN–TCNQ. In addition, there are ionic pairs in AN–TCNQ throughout the temperature range considered. The orbitals of the ionized pair might be stabilized because of one-dimentional fluctuation and reorientational motion of AN. Based on these aspects, the energy diagram of the HT phase is shown in Figure 8a. At room temperature, the dominant carrier is electrons, which are injected into the LUMO of TCNQ because of the relationship between the Fermi level of the electrode and the energy levels of the semiconductor. Thus, the transfer characteristics at room temperature show n-type behavior (Figure 2a). At this temperature, very few holes are injected into the semiconductor crystal. However, the p-type characteristic might be masked by the large n-type contribution. The injected electrons are strongly trapped at ionized and/or crystal defect sites, which cause thermal activation. At this time, the ionized site does not become a hole trap, because molecular orbitals participating in the CT interaction are disordered by reorientational motion of AN. As a result, p-type behavior is uncovered below 250 K (Figure 2b-d). In the IM phase, the reorientational motion of the AN molecule remains. The dominant carrier becomes holes, and the two HOMO levels in Figure 8 represent the two OMs with different transfer energies in the IM phase (Figure 2e). However, energy disorder is lowered, because the nHOMO of AN cannot contribute to hole transport. In the LT phase, reorientational motion stops. The mechanisms of both hole and electron transport follow the hopping model. The carriers are mainly transported on the LUMO of TCNQ because of the relationship between the Fermi level of the electrode and the energy levels of the semiconductor. However, slight hole transport is permitted, because the orbital of the ionic pair changes the trap into a molecular orbital for hole transport (Figure 2f). The large increase of I_{SD} at the transition temperature is caused by an increase of the overlap integral and carrier density associated with the phase transition.

Overall, the AN–TCNQ single-crystal FET with molecular dynamics and charge fluctuation shows drastic changes with decreasing temperature. The results and discussion in this paper might be useful for fabricating devices that can be switching between n-type and p-type. Furthermore, investigation of the device characteristics of the FET has been shown to be a useful method to clarify the band and electronic structures of semiconductor materials.

4. CONCLUSIONS

A FET was fabricated using an AN–TCNQ single crystal, which underwent two phase transitions related to in-plane reorientational motion. The transfer characteristics drastically changed when decreasing the temperature from room temperature to 90 K: n-type → ambipolar-type → p-type → ambipolar-type. The electron and hole transport in the AN–TCNQ FET were different in the HT phase. The electron transport was hopping-type transport, while holes were transported disordered orbital by reorientational motion of AN molecules, which were analyzed

by X-ray diffraction. Ambipolar behavior in the LT phase is considered to be caused by the presence of ionic pairs in the crystal from the optical measurements. The ionic pair became the trap site in the high-temperature region, while it was involved in carrier transport in the low-temperature region.

This work showed that molecular dynamics in crystals can induce drastic changes in device properties. This work also showed that transport characteristics can be used to determine the change of molecular overlap and electronic structure. A detailed study of the FET characteristics is useful for both device design and investigation of the electronic structure or molecular dynamics.

ASSOCIATED CONTENT

Supporting Information

Band calculation; CIF files. This information is available free of charge via the Internet at http://pubs.acs.org.

AUTHOR INFORMATION

Corresponding Author

*E-mail: y-taka@sci.hokudai.ac.jp

*E-mail: inabe@sci.hokudai.ac.jp

Notes

The authors declare no competing financial interest.

ACKNOWLEDGMENT

The authors thank Profs. Y. Hinatsu and M. Wakeshima at Hokkaido University for the use of the magnetic susceptometer, and Prof. S. Takeda and Mr. J. Okamoto at Hokkaido University for help with the DSC measurements. This work was supported in part by a Grant-in-Aid for Scientific Research, Japan Society for the Promotion of Science (JSPS) KAKENHI (No. 26288029) and by the JSPS Core-to-Core Program A, Advanced Research Networks.

REFERENCES

(1) Kaltenbrunner, M.; Sekitani, T.; Reeder, J.; Yokota, T.; Kuribara, K.; Tokuhara, T.; Drack, M.; Schwödiauer, R.; Graz, I.; Bauer-Gogonea, S.; Bauer, S.; Someya, T. An ultra-lightweight design for imperceptible plastic electronics. *Nature* **2013**, 499, 458–463.

(2) Webb, R. C.; Bonifas, A. P.; Behnaz, A.; Zhang, Y.; Yu, K. J.; Cheng, H.; Shi, M.; Bian, Z.; Liu, Z.; Kim, Y.-S.; Yeo, W.-H.; Park, J. S.; Song, J.; Li, Y.; Huang, Y.; Gorbach, A. M.; Rogers, J. A. Ultrathin conformal devices for precise and continuous thermal characterization of human skin. *Nat. Mater.* **2013**, 12, 938–944.

(3) Wang, C.; Dong, H.; Hu, W.; Liu, Y.; Zhu, D. Semiconducting π-Conjugated Systems in Field-Effect Transistors: A Material Odyssey of Organic Electronics. *Chem. Rev.* **2012**, 112, 2208–2267.

(4) Murphy, A. R.; Fréchet, J. M. J. Organic Semiconducting Oligomers for Use in Thin Film Transistors. *Chem. Rev.* **2007**, 107, 1066–1096.

(5) Klauk, H. Organic thin-film transistors. *Chem. Soc. Rev.* **2010**, 39, 2643–2666.

(6) Yi, H. T.; Payne, M. M.; Anthony, J. E.; Podzorov, V. Ultra-flexible solution-processed organic field-effect transistors. *Nat. Commun.* **2012**, 3, 1259.

(7) Okamoto, T.; Mitsui, C.; Yamagishi, M.; Nakahara, K.; Soeda, J.; Hirose, Y.; Miwa, K.; Sato, H.; Yamano, A.; Matsushita, T.; Uemura, T.; Takeya, J. V-shaped organic semiconductors with solution processability, high mobility, and high thermal durability. *Adv. Mater.* **2013**, 25, 6392–6397.

(8) Nakayama, K.; Hirose, Y.; Soeda, J.; Yoshizumi, M.; Uemura, T.; Uno, M.; Li, W.; Kang, M. J.; Yamagishi, M.; Okada, Y.; Miyazaki, E.; Nakazawa, Y.; Nakao, A.; Takimiya, K.; Takeya, J. Patternable solution-crystallized organic transistors with high charge carrier mobility. *Adv. Mater.* **2011**, 23, 1626–1629.

(9) Minemawari, H.; Yamada, T.; Matsui, H.; Tsutsumi, J.; Haas, S.; Chiba, R.; Kumai, R.; Hasegawa, T. Inkjet printing of single-crystal films. *Nature* **2011**, 475, 364–367.

(10) Giri, G.; Verploegen, E.; Mannsfeld, S. C. B.; Atahan-Evrenk, S.; Kim, D. H.; Lee, S. Y.; Becerril, H. A.; Aspuru-Guzik, A.; Toney, M. F.; Bao, Z. Tuning charge transport in solution-sheared organic semiconductors using lattice strain. *Nature* **2011**, 480, 504–508.

(11) Yuan, Y.; Giri, G.; Ayzner, A. L.; Zoombelt, A. P.; Mannsfeld, S. C. B.; Chen, J.; Nordlund, D.; Toney, M. F.; Huang, J.; Bao, Z. Ultra-high mobility transparent organic thin film transistors grown by an off-centre spin-coating method. *Nat. Commun.* **2014**, 5, 3005.

(12) Diao, Y.; Tee, B. C.-K.; Giri, G.; Xu, J.; Kim, D. H.; Becerril, H. a; Stoltenberg, R. M.; Lee, T. H.; Xue, G.; Mannsfeld, S. C. B.; Bao, Z. Solution coating of large-area organic semiconductor thin films with aligned single-crystalline domains. *Nat. Mater.* **2013**, 12, 665–671.

(13) Mitsui, C.; Okamoto, T.; Matsui, H.; Yamagishi, M.; Matsushita, T.; Soeda, J.; Miwa, K.; Sato, H.; Yamano, A.; Uemura, T.; Takeya, J. Dinaphtho[1,2-*b*:2',1'-*d*]chalcogenophenes: Comprehensive Investigation of the Effect of the Chalcogen Atoms in the Phenacene-Type π-Electronic Cores. *Chem. Mater.* **2013**, 25, 3952–3956.

(14) McGarry, K. A.; Xie, W.; Sutton, C.; Risko, C.; Wu, Y.; Young, V. G.; Brédas, J.-L.; Frisbie, C. D.; Douglas, C. J. Rubrene-Based Single-Crystal Organic Semiconductors: Synthesis, Electronic Structure, and Charge-Transport Properties. *Chem. Mater.* **2013**, 25, 2254–2263.

(15) Takahashi, Y.; Hasegawa, T.; Horiuchi, S.; Kumai, R.; Tokura, Y.; Saito, G. High Mobility Organic Field-Effect Transistor Based on Hexamethylenetetrathiafulvalene with Organic Metal Electrodes. *Chem. Mater.* **2007**, 19, 6382–6384.

(16) Takeya, J.; Yamagishi, M.; Tominari, Y.; Hirahara, R.; Nakazawa, Y.; Nishikawa, T.; Kawase, T.; Shimoda, T.; Ogawa, S. Very high-mobility organic single-crystal transistors with in-crystal conduction channels. *Appl. Phys. Lett.* **2007**, 90, 102120.

(17) Kong, H.; Jung, B. J.; Sinha, J.; Katz, H. E. Electrical "Turn-On" Response of Poly(3,3'''-didodecylquaterthiophene) and Electron Donor Blend Transistors to 2,4,6-Trinitrotoluene *Chem. Mater.* **2012**, 24, 2621–2623.

(18) Torsi, L.; Farinola, G. M.; Marinelli, F.; Tanese, M. C.; Omar, O. H.; Valli, L.; Babudri, F.; Palmisano, F.; Zambonin, P. G.; Naso, F. A sensitivity-enhanced field-effect chiral sensor. *Nat. Mater.* **2008**, 7, 412–417.

(19) Rumyantsev, S.; Liu, G.; Shur, M. S.; Potyrailo, R. A.; Balandin, A. A. Selective Gas Sensing with a Single Pristine Graphene Transistor. *Nano Lett.* **2012**, 12, 2294–2298.

(20) Shaymurat, T.; Tang, Q.; Tong, Y.; Dong, L.; Liu, Y. Gas dielectric transistor of CuPc single crystalline nanowire for SO_2 detection down to sub-ppm levels at room temperature. *Adv. Mater.* **2013**, 25, 2269–2273, 2376.

(21) Torsi, L.; Magliulo, M.; Manoli, K.; Palazzo, G. Organic field-effect transistor sensors: a tutorial review. *Chem. Soc. Rev.* **2013**, 42, 8612–8628.

(22) Saito, G.; Yoshida, Y. Development of Conductive Organic Molecular Assemblies: Organic Metals, Superconductors, and Exotic Functional Materials. *Bull. Chem. Soc. Jpn.* **2007**, 80, 1–137.

(23) Ferraris, J.; Cowan, D. O.; Walatka, V.; Perlstein, J. H. Electron transfer in a new highly conducting donor-acceptor complex. *J. Am. Chem. Soc.* **1973**, 95, 948–949.

(24) Jérome, D. Organic Conductors: From Charge Density Wave TTF–TCNQ to Superconducting $(TMTSF)_2PF_6$. *Chem. Rev.* **2004**, 104, 5565–5592.

(25) Takahashi, Y.; Hasegawa, J.; Abe, Y.; Tokura, Y.; Nishimura, K.; Saito, G. Tuning of electron injections for *n*-type organic transistor based on charge-transfer compounds. *Appl. Phys. Lett.* **2005**, 86, 1–3.

(26) Park, S. K.; Varghese, S.; Kim, J. H.; Yoon, S. J.; Kwon, O. K.; An, B. K.; Gierschner, J.; Park, S. Y. Tailor-Made Highly Luminescent and Ambipolar Transporting Organic Mixed Stacked Charge-Transfer Crystals: An Isometric Donor-Acceptor Approach. *J. Am. Chem. Soc.* **2013**, 135, 4757–4764.

(27) Vermeulen, D.; Zhu, L. Y.; Goetz, K. P.; Hu, P.; Jiang, H.; Day, C. S.; Jurchescu, O. D.; Coropceanu, V.; Kloc, C.; McNeil, L. E. Charge Transport Properties of Perylene–TCNQ Crystals: The Effect of Stoichiometry. *J. Phys. Chem. C* **2014**, 118, 24688–24696.

(28) Lefebvre, J.; Odou, G.; Muller, M.; Mierzejewski, A.; Luty, T. Characterization of an orientational disorder in two charge-transfer complexes: anthracene–tetracyanobenzene (A–TCNB) and naphthalene–tetracyanobenzene (N–TCNB). *Acta Crystallogr. Sect. B Struct. Sci.* **1989**, 45, 323–336.

(29) Fyfe, C. A. Molecular Motion in Solid Complexes. Part 1.—π–π Molecular Complexes of Pyrene Studied by Nuclear Magnetic Resonance Spectroscopy. *J. Chem. Soc., Faraday Trans. 2* **1974**, 70, 1633–1641.

(30) Fyfe, C. A.; Harold-Smith, D.; Ripmeester, J. Molecular Motion in Solid π–π Molecular Complexes. Part 3.—Pulse n.m.r. Measurements on Solid Charge-Transfer Complexes of Naphthalene and Pyrene. *J. Chem. Soc., Faraday Trans. 2* **1976**, 72, 2269–2282.

(31) Herbstein, F. H. *Crystalline Molecular Complexes and Compounds*; Oxford University Press: Oxford, U.K., 2005; Vol. 2, Chapter 16.

(32) Williams, R. M.; Wallwork, S. C. Molecular complexes exhibiting polarization bonding. XI. The crystal and molecular structure of the 7,7,8,8-tetracyanoquinodimethane-anthracene complex. *Acta Crystallogr. Sect. B Struct. Crystallogr. Cryst. Chem.* **1968**, 24, 168–174.

(33) Sheldrick, G. M. A short history of *SHELX*. *Acta Crystallogr., Sect. A* **2008**, 64, 112–122.

(34) Hoffmann, R. An Extended Hückel Theory. I. Hydrocarbons. *J. Chem. Phys.* **1963**, 39, 1397.

(35) Whangbo, M.-H.; Hoffmann, R.; Woodward, R. B. Conjugated One and Two Dimensional Polymers. *Proc. R. Soc. A Math. Phys. Eng. Sci.* **1979**, 366, 23–46.

(36) Ren, J.; Liang, W.; Whangbo, M.-H. *CAESAR*; Prime-Color Software, Inc.: Raleigh, NC, 1998.

(37) Frisch, M. J.; Trucks, G. W.; Schlegel, H. B.; Scuseria, G. E.; Robb, M. A.; Cheeseman, J. R.; Scalmani, G.; Barone, V.; Mennucci, B.; Petersson, G. A.; Nakatsuji, H.; Caricato, M.; Li, X.; Hratchian, H. P.; Izmaylov, A. F.; Bloino, J.; Zheng, G.; Sonnenberg, J. L.; Hada, M.; Ehara, M.; Toyota, K.; Fukuda, R.; Hasegawa, J.; Ishida, M.; Nakajima, T.; Honda, Y.; Kitao, O.; Nakai, H.; Vreven, T.; Montgomery, J. A., Jr; Peralta, J. E.; Ogliaro, F.; Bearpark, M.; Heyd, J. J.; Brothers, E.; Kudin, K. N.; Staroverov, V. N.; Kobayashi, R.; Normand, J.; Raghavachari, K.; Rendell, A.; Burant, J. C.; Iyengar, S. S.; Tomasi, J.; Cossi, M.; Rega, N.; Millam, N. J.; Klene, M.; Knox, J. E.; Cross, J. B.; Bakken, V.; Adamo, C.; Jaramillo, J.; Gomperts, R.; Stratmann, R. E.; Yazyev, O.; Austin, A. J.; Cammi, R.; Pomelli, C.; Ochterski, J. W.; Martin, R. L.; Morokuma, K.; Zakrzewski, V. G.; Voth, G. A.; Salvador, P.; Dannenberg, J. J.; Dapprich, S.; Daniels, A. D.; Farkas, Ö.; Foresman, J. B.; Ortiz, J. V.; Cioslowski, J.; Fox, D. J. Gaussian 09, Revision C.01; Gaussian, Inc.: Wallingford, CT, **2010**.

(38) Bain, G. A.; Berry, J. F. Diamagnetic Corrections and Pascal's Constants. *J. Chem. Educ.* **2008**, 85, 532.

(39) Wright, J. D. *Molecular Crystals*, 2nd ed.; Cambridge University Press: Cambridge, U.K., 1995.

(40) Kistenmacher, T. J.; Emge, T. J.; Bloch, A. N.; Cowan, D. O. Structure of the red, semiconducting form of 4,4',5,5'-tetramethyl-Δ2,2'-bi-1,3-diselenole-7,7,8,8-tetracyano-p-quinodimethane, TMTSF–TCNQ. *Acta Crystallogr. Sect. B Struct. Crystallogr. Cryst. Chem.* **1982**, 38, 1193–1199.

(41) Torrance, J. B.; Vazquez, J. E.; Mayerle, J. J.; Lee, V. Y. Discovery of a Neutral-to-Ionic Phase Transition in Organic Materials. *Phys. Rev. Lett.* **1981**, *46* (4), 253–257.

(42) Jonkman, H. T.; Kommandeur, J. The UV spectra and their calculation of TCNQ and its mono- and di-valent anion. *Chem. Phys. Lett.* **1972**, 15, 496–499.

(43) Chappell, J. S.; Bloch, A. N.; Bryden, W. A.; Maxfield, M.; Poehler, T. O.; Cowan, D. O. Degree of charge transfer in organic conductors by infrared absorption spectroscopy. *J. Am. Chem. Soc.* **1981**, 103, 2442–2443.

(44) Okamoto, H.; Tokura, Y.; .Koda, T. Optical study of structural phase transition in organic charge-transfer crystals K- and Rb-tetracyanoquinodimethane. *Phys. Rev. B* **1987**, 36, 7, 3858-3867.

(45) Szu, S. M. *Semiconductor Devices: Physics and Technology*; 1985.

(46) Bässler, H. Charge Transport in Disordered Organic Photoconductors a Monte Carlo Simulation Study. *Phys. status solidi* **1993**, 175, 15–56.

.

Insert Table of Contents artwork here